

Transport of energetic electrons into Saturn's inner magnetosphere

C. Paranicas,¹ D. G. Mitchell,¹ E. Roussos,² P. Kollmann,² N. Krupp,² A. L. Müller,^{2,3}
S. M. Krimigis,¹ F. S. Turner,¹ P. C. Brandt,¹ A. M. Rymer,¹ and R. E. Johnson⁴

Received 22 June 2010; revised 9 August 2010; accepted 16 August 2010; published 22 September 2010.

[1] We present energetic electron data obtained by Cassini's Magnetospheric Imaging Instrument in the inner magnetosphere of Saturn. We find here that inward transport and energization processes are consistent with conservation of the first two adiabatic invariants of motion. We model several injections near local midnight, one injection has a maximum energy of hundreds of keV, that are consistent with data. We also present mission-averaged data that shows an injection boundary in radial distance. Inward of this boundary, fluxes fall off toward the planet. Around this inner boundary, strong local time asymmetries are present in the averaged data with peak fluxes near midnight.

Citation: Paranicas, C., et al. (2010), Transport of energetic electrons into Saturn's inner magnetosphere, *J. Geophys. Res.*, 115, A09214, doi:10.1029/2010JA015853.

1. Introduction

[2] Saturn's inner magnetosphere ($L < 10$) contains stably trapped distributions of energetic ions and electrons in the energy range above 1 MeV [e.g., *Simpson et al.*, 1980; *Krupp et al.*, 2009]. Just below this energy range, in the tens of keV to 1 MeV, the inner magnetosphere does not appear to be uniformly filled. That is, discrete populations of energized particles (hereafter referred to generally as injections) are observed superimposed on background fluxes of various levels. This is especially striking in energetic protons [*Paranicas et al.*, 2008]. Below about 200 keV, these particles undergo strong losses via charge exchange in the dense neutral gas [e.g., *Melin et al.*, 2009]. Observations of the inner magnetosphere show that fluxes of these particles are very low, except for recent injections.

[3] Because of ion losses via charge exchange, it is easy to understand why some ion species over a range of energies would be nearly absent in the inner magnetosphere of Saturn. However, data indicate that the inner magnetosphere is not uniformly filled with electrons in the tens to hundreds of keV energy range either. Instead, recent injections and even aging injections are observed to have the highest intensities [*Mauk et al.*, 2005; *Paranicas et al.*, 2007; *Müller et al.*, 2010]. In this paper, we will examine how deeply into the inner magnetosphere energetic electron injections penetrate, how they evolve and how they populate that region. We will also examine the relationship between injected electrons and trapped electrons near 1 MeV.

[4] Data presented in this paper are from Cassini's Magnetospheric Imaging Instrument (MIMI). This instrument is described in detail by *Krimigis et al.* [2004]. MIMI has three separate sensors but since we are focusing on electrons, we will consider data from the Low Energy Magnetospheric Measurement System (LEMMS) only. LEMMS measures electrons in the energy range from about 20 keV to tens of MeV in discrete energy bands with high time resolution (about 3 s to 24 s). Because we wish to examine pulse-height-analyzed (PHA) data, the energy range of our study is limited to 20 keV to 1.7 MeV.

[5] Beginning on about day 2009–285, many Cassini orbits began to be very equatorial (some within 1° of the equator) for large regions around periapsis. Except for the mission-averaged data, we will focus here on data obtained after that date. Equatorial passes are very advantageous for studying trapped particles because all of these particles must pass through the magnetic equator in their bounce motion. In subsequent sections, we consider typical distributions in the inner magnetosphere, a specific orbit in detail, and summary data, looking at the radial injection boundary and losses.

2. Energetic Electrons in the Inner Magnetosphere

[6] In this section, we will give an overview of the electron data around a typical Saturn periapsis. Figure 1 shows an example of 20 keV to about 1.7 MeV electron intensities observed by LEMMS on days 2010–169 and 2010–170. Injections of various ages can be identified in this plot. A series of recent (nearly vertical) injections can be seen just after the beginning of day 2010–170, below 100 keV. A series of bands representing time-dispersed populations can be identified on the left-hand side of the plot extending up to energies of hundreds of keV. Aside from instrument background (vertical intensifications near the center of the plot), there appears to be a radial limit of injected flux, especially in the hundreds of keV energy range. There are at least two possible reasons for this. One is that there is an approximate

¹Johns Hopkins University Applied Physics Laboratory, Laurel, Maryland, USA.

²Max-Planck-Institut für Sonnensystemforschung, Katlenburg-Lindau, Germany.

³Institute of Geophysics and Meteorology, University of Cologne, Cologne, Germany.

⁴Engineering Physics, University of Virginia, Charlottesville, Virginia, USA.

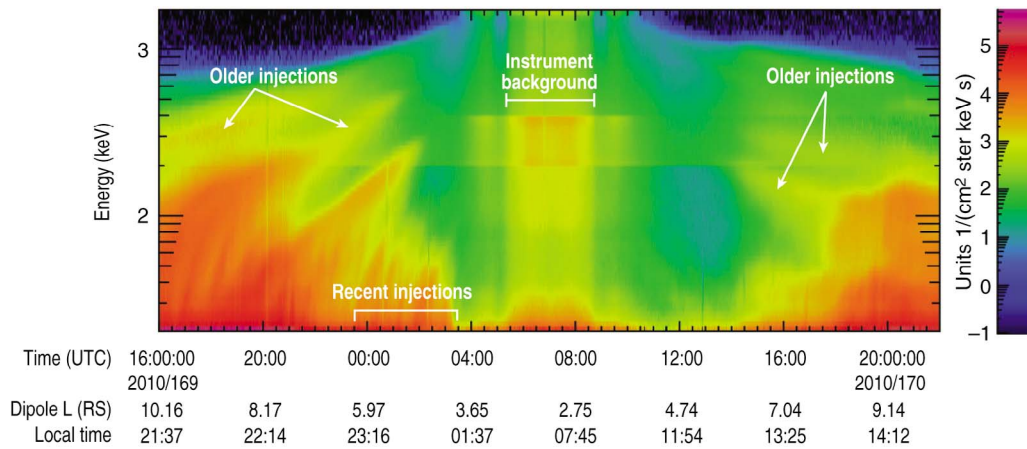


Figure 1. Spectrogram of electron intensity (color) as a function of time and spacecraft L shell (on the horizontal axis) and log energy (vertical axis). Data are from 2010–169 16:00 UTC through 2010–170 22:00 UTC. The vertical stripes near the center of the plot are due to background. The horizontal discontinuity between 200 and 400 keV is due to a change in detector.

inner injection boundary in L-shell. Furthermore, injections to these energies appear to be most common around midnight [Müller *et al.*, 2010]. The other is that inward of $L \sim 5$, the scattering and energy loss of energetic electrons in the gas/grain environment limits the survival times of these particles.

[7] Near the top of Figure 1, there is a sharp transition in intensity from trapped flux to lower, cosmic ray background levels. This sharp transition increases in energy with decreasing L-shell. In Figure 2, we examine the upper energy edge of the trapped population more quantitatively. We focus on data obtained on the inbound portion of the period shown in Figure 1. For these data, Cassini remained within about 2° of the planet's equatorial plane and sampled particles with local pitch angles $< 45^\circ$. The symbols represent an estimate

of the energy corresponding to the edge of the trapped population. This is approximately where intensity drops below the value one count per $\text{cm}^2\text{-s}\cdot\text{sr}\cdot\text{keV}$. The energy resolution is dictated by the spacing (see the step-like features in the symbols of the plot). For comparison, the solid line corresponds to an energization curve in which the first two (relativistic) adiabatic invariants of motion (hereafter μ and J) are held fixed [Kaufmann, 1965]. The invariants are calculated assuming the values $E = 1.546$ MeV and $\alpha_{\text{eq}} = 16^\circ$ at $L = 4.3$.

[8] Figure 2 suggests that processes of inward transport approximately conserve μ and J . Dialynas *et al.* [2009], for instance, found a similar energization organized the proton data following injections. Discrepancies between the data

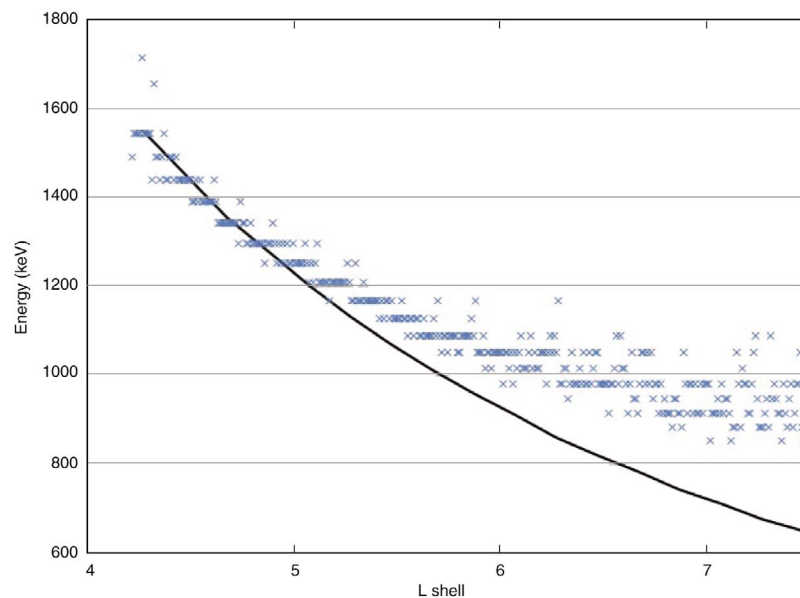


Figure 2. Edge of trapped radiation (x's) as a function of dipole L-shell (horizontal axis) and energy in keV (vertical axis). Data were analyzed from the inbound portion of the periapsis period shown in Figure 1. The solid line shows a curve corresponding to the conservation of relativistic μ and J .

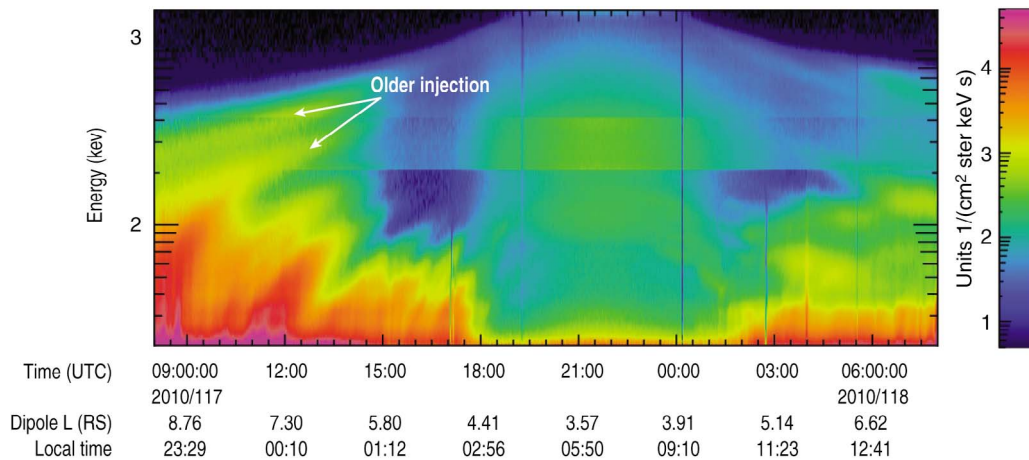


Figure 3. Same spectrogram design as in Figure 1 for LEMMS PHA electron data obtained on days 2010 117–118. Here LEMMS is detecting local pitch angles of about 60° for the entire time period.

and dipole energization curve can occur for a variety of reasons. For example, the presence of a newer feature that extends in with high intensity to at least $L = 7.1$ (22:00 UTC) would not be expected to join smoothly with a dispersed older population or populations at these distances. Each injected population has a maximum μ value that is governed by the source population's location and maximum energy. It is not expected that these would be same each time.

[9] At energies above the edge, the instrument is measuring a level of flux that is due to cosmic rays. We find that the edge between the trapped flux and the cosmic ray flux is not always in the same place from orbit to orbit. The location in energy of the trapped particle boundary likely depends on the superposition of past injections. These come from different distances and source populations. We discuss this further in the sections that follow.

3. Injection Model

[10] In Figure 3, we show another example of a LEMMS electron spectrogram, this time from the period 2010–117 08:00 UTC through 2010–118 08:00 UTC. We chose these data for analysis because, for the entire time period, the spacecraft was less than one half of one degree from the magnetic equator and LEMMS was measuring pitch angles of approximately 60° . This means all the particles detected during this time period have the same drift speed. This plot shows a combination of recent and older injections that we would like to consider more carefully in this section.

[11] In a previous paper, we simulated the features in a MIMI time-energy spectrogram using a simple model of the injection [Paranicas et al., 2007]. There we assumed a single longitude would be populated over a wide range of L shells, energies, and equatorial pitch angles. After such an injection, particle guiding-centers would move in longitude at a rate based on an approximation to the L -dependent corotation speed [Mauk et al., 2005] and the gradient-curvature drift speed [e.g., Thomsen and Van Allen, 1980]. Depending on the energy and pitch angle LEMMS was sampling at each time, points would be plotted if some subset of the energies and pitch angles in the initial injection were at the same location as the spacecraft.

[12] In the previous section, we saw that the upper energy cutoff of the trapped particles could be approximated using the conservation of μ and J . We have therefore modified our 2007 model slightly: we now populate each L shell with all energies up to an L -dependent maximum. This maximum energy is computed for a single μ and J . This change in our simulation mostly affects the appearance of the high-energy portion of the model spectrogram. Most importantly, with a cutoff, there are fewer re-encounters by the spacecraft of old injections at high energy. We also now focus on injections initiated near local midnight.

[13] In Figure 4, we show the results of the model that includes three separate injections. The color of the lines in our model represents an ordering by injection age: orange, yellow, green, blue (youngest to oldest). The injection near the left hand side of the plot in orange (observed near 2010–117 09:00 UTC) was launched in our model at 2010–117 07:12 UTC at about 21:30 LT to 130 keV. The spacecraft re-encounters a low-energy portion of this injection between hours 26 and 31. The second small injection that appears in yellow (observed between about 2010–117 12:00 and 14:00 UTC) was initiated in our model on day 2010–116 at 06:00 UTC, near midnight local time, also to 130 keV. The spacecraft re-encounters a portion of this injection between 19 and 29 h. These arcs are typical features observed near spacecraft periapses, both in the data (Figure 3) and in our simulation. These two injections are used to help clarify fragments that are not part of the injection to hundreds of keV described next.

[14] The injection to the highest energies in our model was initiated just over an hour before midnight local time on day 2010–115 07:12 UTC inward to a distance of $L \sim 5.8$. Any features in the simulation not mentioned in the previous paragraph belong to this single injection. We do not model the injections in Figure 3 with maximum energies below about 100 keV. The choice of inner radial edge for this injection was governed by the data. Just after about 2010–117 15:00 UTC ($L \sim 5.8$) in Figure 3, several injection bands decrease rapidly in intensity. We chose the maximum energy of this injection to be 700 keV at $L = 5.8$. For electrons, this energy corresponds to $\gamma \sim 2.37$ and $\mu \sim 821$ MeV/G; here $\gamma = (1 - \beta^2)^{-1/2}$

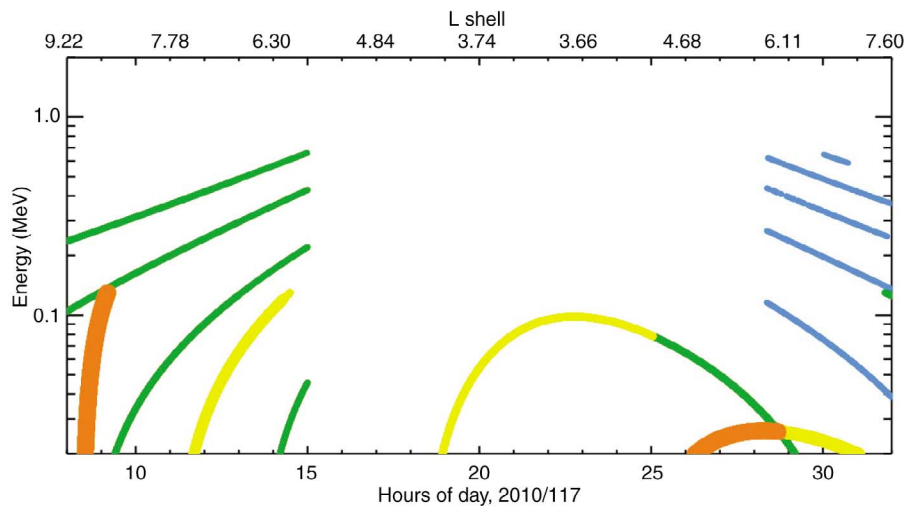


Figure 4. Simulation of Figure 3 data using 3 separate injections initiated near midnight. The horizontal axis is time in hours since the beginning of day 2010–117. The vertical axis is energy and the upper horizontal axis shows the L-shell of Cassini. Points are plotted in color representing their approximate age range since injection with orange, yellow, green, blue from youngest to oldest.

and $\beta = v/c$. Using this μ , we populate $L > 5.8$ so that, for instance, $L = 10$ is populated with energies up to 207 keV.

[15] As Figure 4 shows, the fragments in Figure 3 can be organized together by their parent events in a way that is not obvious without modeling. Most notably, the bands that reach the highest energies during the inbound portion of the trajectory seem to be linked to each other and other features. Since the main injection in this plot is more than 24 h old, it is possible that this type of event is much less frequent than the injections that have maximum energies near and below 100 keV. It is also possible that this kind of event is connected to the large-scale injection of ions that is inferred from energetic neutral atom (ENA) imaging [e.g., *Mitchell et al.*, 2009]. We discuss these possibilities below.

[16] The disagreement between the data and the simulation is greatest on the dayside (right-hand side of the plot). These are the oldest remnants of the injections and it makes sense that they have the least coherence. Electrons disperse on the drift shells, scatter and lose energy in the medium of the gas and grains. Also, Cassini data have revealed asymmetries in particle drift paths close to the planet [e.g., *Roussos et al.*, 2007] that can reduce the organization of the bands.

4. Injection Boundary and Losses

[17] In this section we consider the effects of the electron injection process over much longer time periods. In Figure 5, we show a mission-averaged summary of 41–60 keV electron intensities organized by dipole L-shell and local time. Measured local pitch angle is transformed to equatorial pitch angle using a dipolar model of the magnetic field. Intensities corresponding to equatorial pitch angles between 50° and 130° are considered. We chose this pitch angle range over a narrower one to improve statistics. Data obtained when the sensor was pointing in the direction of the sun have been removed because the light diffuses and causes problems.

[18] Electrons near ~ 50 keV orbit Saturn at a rate that is close to the corotation speed of the plasma [e.g., *Thomsen and*

Van Allen, 1980]. Therefore, it is noteworthy that there are strong local-time asymmetries in the most intense fluxes, especially inward of $L \sim 8$. *Carbary et al.* [2009] showed data similar to that presented in Figure 5 for fluxes of hundreds of keV electrons. In Carbary’s work, the 110–365 keV electron distributions in local time and L-shell resemble the pattern shown in Figure 5. The main difference between the two energy ranges is the extent of the most intense fluxes in L. In Figure 5, the most intense fluxes reach in to about $L = 5.5$ (near midnight) and about $L = 8$ (around noon). In Carbary’s work, the most intense fluxes are high to about $L = 5$ near midnight and $L = 7$ near noon. This is consistent with injection processes around midnight that conserve adiabatic invariants.

[19] After these electrons are injected to $L \sim 5$, they begin to disperse and also encounter high densities of neutral gas and grains. As several analyses have shown [*Richardson*, 1998; *Melin et al.*, 2009; *Cassidy and Johnson*, 2010], total neutral gas densities become significant inward of $8 R_S$. Neutral gas will affect trapped tens to hundreds of keV electrons in a number of ways. Electrons passing into materials will scatter and lose energy. *Zombeck* [1982] gives a version of a standard formula for an incident electron’s energy loss to ionization and excitation of the atoms in a medium as,

$$\frac{dE}{dx} = (10^{-24} \text{ cm}^2) \frac{mc^2}{\beta^2} NZ \left[\ln \left[\beta \sqrt{\frac{E}{mc^2}} \left(\frac{E + mc^2}{I} \right) \right] - \frac{\beta^2}{2} \right] \quad (1)$$

Here mc^2 is the electron rest mass and E is the incident particle’s kinetic energy. The properties of the gas or grain target are: $N = \text{atoms/cm}^3$, $Z = \text{atomic number}$, and I is the mean ionization potential. This dE/dx is a falling function in energy, reaching a minimum around 1 MeV. Above that energy, processes such as bremsstrahlung and synchrotron radiation become more important.

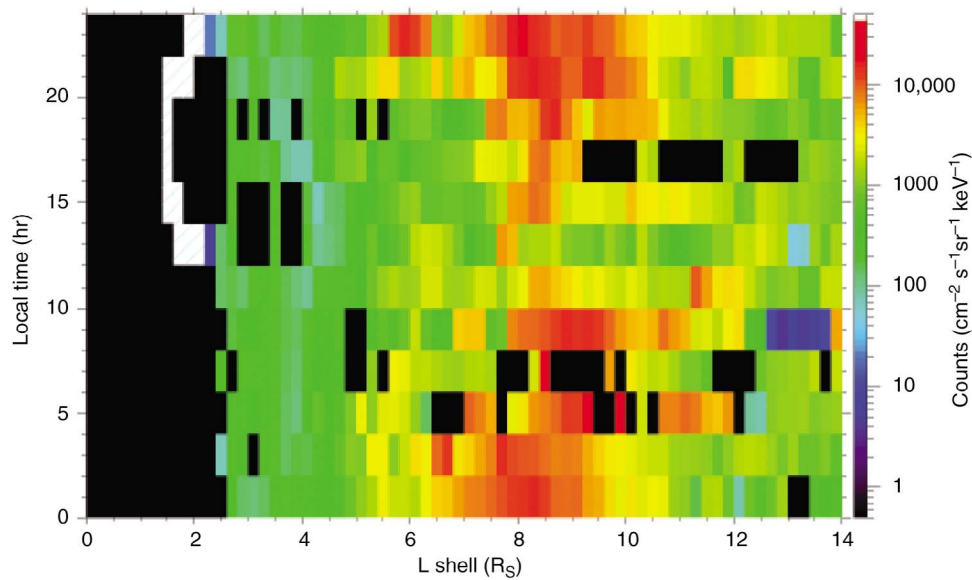


Figure 5. Intensity of 41–60 keV electrons (color) with equatorial pitch angles between 50° – 130° . LEMMS data are converted to equatorial pitch angle using a dipole magnetic field model. The data are then averaged and binned by dipole L-shell and local time (hours). Data include the time period from day 2004–182 to day 2010–155.

[20] Equation (1) suggests energy loss per unit length is proportional to the number of electrons per unit volume in the target material ($= NZ$). Neutral gas is escaping from Enceladus with several times the mass of the grains (see, for instance, discussion in *Spencer et al.* [2009]). Therefore energetic electrons passing through a medium with the same gas/grain mass ratio found in the escaping population would lose more energy, on average, to the gas. Using O and OH gas densities near Enceladus given by *Melin et al.* [2009], we find a 30 keV electron loses 1 keV in about 90 h.

[21] In the excitation of atoms in a medium, the electron velocity vector changes in both size and direction. *Moncrieff et al.* [1979] considered both the elastic and inelastic scattering of 25 keV electrons in N_2 gas. From their work and the oxygen densities reported by *Melin et al.* [2009] near Enceladus, the probability of scattering by more than 2° reaches 1/2 in roughly 40 h. This is based on a half bounce time of 5 s (for a 25 keV electron at $L = 5$ with a mirror latitude of 10°) during which we assume the electron passes through about 60,330 km of gas. Scattering of the electrons increases their chances of entering the planetary loss cone. Therefore both scattering and gradual energy loss limit the lifetimes of these particles in the gas/grain environment.

5. Discussion

[22] Previously *Mitchell et al.* [2009] described a recurrent energization process in energetic ions. They suggested that dipolarization in the tail would lead to an active quadrant between midnight and dawn. This active quadrant would repeatedly energize very extended populations of ions inward to about 12–15 R_S . Those authors point out that the effects of this energization processes could be seen as close in as 7 R_S . One way to interpret this is that spatially confined populations can be energized closer to the planet due to processes farther

out in radial distance. It is likely that the injections to hundreds of keV that we are modeling above are the electron counterparts to these processes. It is striking that the energizations described here can affect L-shells as far in as 5.8 R_S .

[23] We have not yet seen data in which direct energizations (nearly vertical structures in the time-energy spectrograms) to energies of 1 MeV occur close to the planet ($L \sim 4$); although we cannot completely rule out local time sampling bias of the spacecraft. Therefore, we suggest that electrons observed at and above about 1 MeV close to the planet do not result from direct injections to these energies and distances. Instead, we hypothesize that there are initial injections to the hundreds of keV to minimum distances of about $L = 5$. If this stage of the energization process is due to interchange [e.g., *Chen and Hill*, 2008], this must be followed by a secondary process to raise the energy to the MeV range. Our analysis of the energy edge between the trapped particle and cosmic ray flux levels suggests that this secondary process also conserves μ and J . Therefore, we propose that radiation belt electrons get energized by a two-step process.

[24] If the energization process in electrons is similar to what *Mitchell et al.* [2009] describe for ions, it would explain the inner radial boundary of electron fluxes. Data presented above and those shown by *Carbary et al.* [2009] indicate fluxes peak in the range $L = 5$ to $L = 8$ (depending on the local time and energy). We suggest this approximately tracks the influence of recurrent energization processes between midnight and dawn that occur farther out. Furthermore, some level of loss away from midnight would be expected if electrons, once injected, undergo scattering and energy loss in the gas/grain environment. This may qualitatively describe the survey plots, but more quantitative analyses of how electrons scatter and lose energy will be pursued in future work.

[25] **Acknowledgments.** The first author would like to thank R. B. Decker, H. T. Smith, J. Vandegriff, M. Kusterer and G. Stephens, all at APL. This work was partially supported by grants between NASA and the Johns Hopkins University.

[26] Masaki Fujimoto thanks George Hospodarsky and another reviewer for their assistance in evaluating this paper.

References

- Carbary, J. F., D. G. Mitchell, N. Krupp, and S. M. Krimigis (2009), L shell distribution of energetic electrons at Saturn, *J. Geophys. Res.*, *114*, A09210, doi:10.1029/2009JA014341.
- Cassidy, T. A., and R. E. Johnson (2010), Collisional spreading of Enceladus's neutral cloud, *Icarus*, doi:10.1016/j.icarus.2010.04.010, in press.
- Chen, Y., and T. W. Hill (2008), Statistical analysis of injection/dispersion events in Saturn's inner magnetosphere, *J. Geophys. Res.*, *113*, A07215, doi:10.1029/2008JA013166.
- Dialynas, K., S. M. Krimigis, D. G. Mitchell, D. C. Hamilton, N. Krupp, and P. C. Brandt (2009), Energetic ion spectral characteristics in the Saturnian magnetosphere using Cassini/MIMI measurements, *J. Geophys. Res.*, *114*, A01212, doi:10.1029/2008JA013761.
- Kaufmann, R. L. (1965), Conservation of the first and second adiabatic invariants, *J. Geophys. Res.*, *70*, 2181–2186, doi:10.1029/JZ070i009p02181.
- Krimigis, S. M., et al. (2004), Magnetosphere imaging instrument (MIMI) on the Cassini mission to Saturn/Titan, *Space Sci. Rev.*, *114*, 233–329, doi:10.1007/s11214-004-1410-8.
- Krupp, N., et al. (2009), Energetic particles in Saturn's magnetosphere during the Cassini nominal mission (July 2004–July 2008), *Planet. Space Sci.*, doi:10.1016/j.pss.2009.06.010.
- Mauk, B. H., et al. (2005), Energetic particle injections in Saturn's magnetosphere, *Geophys. Res. Lett.*, *32*, L14S05, doi:10.1029/2005GL022485.
- Melin, H., D. E. Shemansky, and X. Liu (2009), The distribution of atomic hydrogen and oxygen in the magnetosphere of Saturn, *Planet. Space Sci.*, doi:10.1016/j.pss.2009.04.014.
- Mitchell, D. G., et al. (2009), Recurrent energization of plasma in the midnight-to-dawn quadrant of Saturn's magnetosphere, *Planet. Space Sci.*, doi:10.1016/j.pss.2009.04.002.
- Moncrieff, D. A., P. R. Barker, and V. N. E. Robinson (1979), Electron scattering by gas in the scanning electron microscope, *J. Phys. D Appl. Phys.*, *12*, 38–49, doi:10.1088/0022-3727/12/4/005.
- Müller, A. L., J. Saur, N. Krupp, E. Roussos, B. H. Mauk, A. M. Rymer, D. G. Mitchell, and S. M. Krimigis (2010), Azimuthal plasma flow in the Kronian magnetosphere, *J. Geophys. Res.*, *115*, A08203, doi:10.1029/2009JA015122.
- Paranicas, C., et al. (2007), Energetic electrons injected into Saturn's neutral gas cloud, *Geophys. Res. Lett.*, *34*, L02109, doi:10.1029/2006GL028676.
- Paranicas, C., et al. (2008), Sources and losses of energetic protons in Saturn's magnetosphere, *Icarus*, *197*, 519–525, doi:10.1016/j.icarus.2008.05.011.
- Richardson, J. D. (1998), Thermal plasma and neutral gas in Saturn's magnetosphere, *Rev. Geophys.*, *36*, 501–524, doi:10.1029/98RG01691.
- Roussos, E., et al. (2007), Electron microdiffusion in the Saturnian radiation belts: Cassini MIMI/LEMMS observations of energetic electron absorption by the icy moons, *J. Geophys. Res.*, *112*, A06214, doi:10.1029/2006JA012027.
- Simpson, J. A., T. S. Bastian, D. L. Chenette, R. B. McKibben, and K. R. Pyle (1980), The trapped radiations of Saturn and their absorption by satellites and rings, *J. Geophys. Res.*, *85*, 5731–5762, doi:10.1029/JA085iA11p05731.
- Spencer, J. R., et al. (2009), Enceladus: An active cryovolcanic satellite, in *Saturn From Cassini-Huygens*, edited by M. K. Dougherty, L. W. Esposito, and S. M. Krimigis, pp. 683–724, Springer, Dordrecht, Netherlands, doi:10.1007/978-1-4020-9217-6_21.
- Thomsen, M., and J. A. Van Allen (1980), Motion of trapped electrons and protons in Saturn's inner magnetosphere, *J. Geophys. Res.*, *85*, 5831–5834, doi:10.1029/JA085iA11p05831.
- Zombeck, M. V. (1982), *Handbook of Space Astronomy and Astrophysics*, Cambridge Univ., Cambridge, U. K.

P. C. Brandt, S. M. Krimigis, D. G. Mitchell, C. Paranicas, A. M. Rymer, and F. S. Turner, Johns Hopkins University Applied Physics Laboratory, MS MP3-E128, 11100 Johns Hopkins Rd., Laurel, MD 20723, USA. (chris.paranicas@jhuapl.edu)

R. E. Johnson, Engineering Physics, University of Virginia, Charlottesville, VA 22903, USA.

P. Kollmann, N. Krupp, A. L. Müller, and E. Roussos, Max-Planck-Institut für Sonnensystemforschung, Max-Planck-Str. 2, Katlenburg-Lindau D-37191, Germany.